Density Functional Theory Study of CO Adsorption on Molybdenum Sulfide

ARTICLE *in* THE JOURNAL OF PHYSICAL CHEMISTRY B · MARCH 2005

Impact Factor: 3.3 · DOI: 10.1021/jp046646l · Source: PubMed

5 AUTHORS, INCLUDING:

Tao Zeng
Carleton University
41 PUBLICATIONS **295** CITATIONS
SEE PROFILE

Xiao-Dong Wen
Institute of Coal Chemsitry, Chinese Academ…
99 PUBLICATIONS **937** CITATIONS
SEE PROFILE

Yong-Wang Li
Chinese Academy of Sciences
405 PUBLICATIONS **6,057** CITATIONS
SEE PROFILE

Density Functional Theory Study of CO Adsorption on Molybdenum Sulfide

Tao Zeng,[†] Xiao-Dong Wen,[†] Gui-Sheng Wu,[†] Yong-Wang Li,*[,†] and Haijun Jiao*[,†,‡]

State Key Laboratory of Coal Conversion (SKLCC), Institute of Coal Chemistry, Chinese Academy of Science, Taiyuan, Shanxi 030001, China and Leibniz-Institut für Organische Katalyse an der Universität Rostock e.V., Buchbinderstrasse 5-6, 18055 Rostock, Germany

Received: July 28, 2004; In Final Form: November 18, 2004

CO adsorption on four MoS_x (stoichiometric and nonstoichiometric) clusters has been investigated by using density functional method. It is found that CO prefers adsorption on the coordinatively unsaturated $(10\bar{1}0)$ surface. The adsorption energy of high coverage shows the additivity as compared with that of one CO adsorption, and there is no significant repulsive interaction between the end-on adsorbed CO probes. The computed CO stretching frequencies (2000−2080 cm^{-1}) agree perfectly with the experimental data (a broad band centered at 2070 cm^{-1} with a tail extent to 2000 cm^{-1}). No bridged CO adsorption is favored energetically under high CO concentration, and this might explain the catalytic ability of MoS_x for C_1 products instead of higher hydrocarbons and alcohols.

Introduction

Molybdenum sulfide (MoS_2, more precisely MoS_x) is a widely used catalyst in CO hydrogenation (HYD) and hydrodesulfurization processes for the production of cleaner fuels.[1] In contrast to metallic catalysts, MoS_2 has the advantage of excellent resistance to sulfur poisoning. In CO HYD, molecular COs are first adsorbed on the MoS_x surfaces and then participate in the elementary reaction steps to yield the products. Therefore, identification of the key steps and understanding of the energetic and structural properties of the intermediates might benefit the discovery of the whole CO HYD process on catalysts and, in turn, the synthesis of more effective catalysts for the reaction.

Despite the extensive experimental work on synthesis of hydrocarbons and alcohols as well as adsorption of CO on MoS_x, no general agreement about the detailed reaction mechanism has been archived because of the difficulty to get the microscopic knowledge under the real experimental conditions. On the other hand, the MoS_x surfaces will change or reconstruct during the reaction, and so does the CO adsorption on them. The changes of surface structures and compositions make the systematic study and understanding of the catalytic process difficult and problematic. It also is well-known experimentally that the coordinatedly unsaturated Mo sites on the reduced surfaces play the key role for CO adsorption and activation; for example, the more reduced the site, the stronger the CO activation and adsorption. Sung and Hoffman[2] theoretically analyzed CO adsorption on transition metal surface and emphasized the synergetic donation and back-donation between CO and metal as the most important interaction. Pavão et al.[3] showed that the interaction between metal surface and CO might lead to breaking and forming chemical bonds, and they emphasized the importance of the precursor tilted state in CO dissociation on metal surfaces under the consideration of surface interaction and orientation models.

MoS_x catalysts from different synthetic methods have diverse surface structures, as reflected by the surface S atoms. Theoretical studies show that the number of sulfur atoms on the edges of MoS_x depends on the H_2/H_2S molar ratio and that the number of surface sulfur atoms decreases with the increase of H_2 partial pressure.[4] Two kinds of $(10\bar{1}0)$ surfaces (100 and 50% sulfur coverage) and two kinds of $(\bar{1}010)$ surfaces (100 and 50% sulfur coverage) can stably exist under different H_2 pressures. These surfaces should adsorb CO in different ways.[5]

Because of the change of surface structures and composition of the MoS_x catalyst, it is desired and necessary to study CO adsorption on each kind of surface using different MoS_x clusters, and this enables a better and systematic comparison between theory and experiments.

On the basis of DFT computation on a nonstoichiometric sulfur surface, Travert et al.[5] assigned the observed IR frequencies to different adsorption modes. However, they could not identify the adsorption differences between the corner and side, as suggested by Müller et al.[6] and Elst et al.[7] Generally, there is a sharp peak at 2100 cm^{-1} and a broad band at 2070 cm^{-1} with a tail extent to 2000 cm^{-1} in the IR spectra of adsorbed CO on MoS_x.[6−8] It has been generally believed that this band is attributed to CO adsorbed on 4-fold coordinated Mo[9] and that it is responsible for HYD. Compared with 2143 cm^{-1} of free CO, Maugé et al. attributed this red-shift to the back-donation from surface.[10] Furthermore, Maugé et al. compared the adsorbed CO IR spectra between supported and unsupported MoS_x and found that the near 2100 cm^{-1} peak emerged only in the supported rather in the unsupported sample. They attributed this phenomenon to a specific poisoning of Mo sites, while Tsyganenko et al.[11] attributed this shift to the different oxidation states of molybdenum in MoS_x. On the basis of an X-ray photoelectron spectroscopy (XPS) study of MoS_2 exposed to CO, Iranmahboob et al.[12] found that CO was adsorbed on the surface of MoS_2 rather than MoS_3 and that MoS_2 may be a good catalyst for methanation. Jaworowski et al.[13] studied the CO dissociation on Mo (110) by high-resolution core-level spectroscopy and preliminary near-edge X-ray adsorption fine structure, and they found that the higher the CO coverage, the higher the temperature for CO dissociation and ascribed this

* Corresponding authors. E-mail: hjiao@ifok.uni-rostock.de; ywl@sxicc.ac.cn.
† Chinese Academy of Science.
‡ Leibniz-Institut für Organische Katalyse an der Universität Rostock.

10.1021/jp046646l CCC: $30.25
Published on Web 01/26/2005

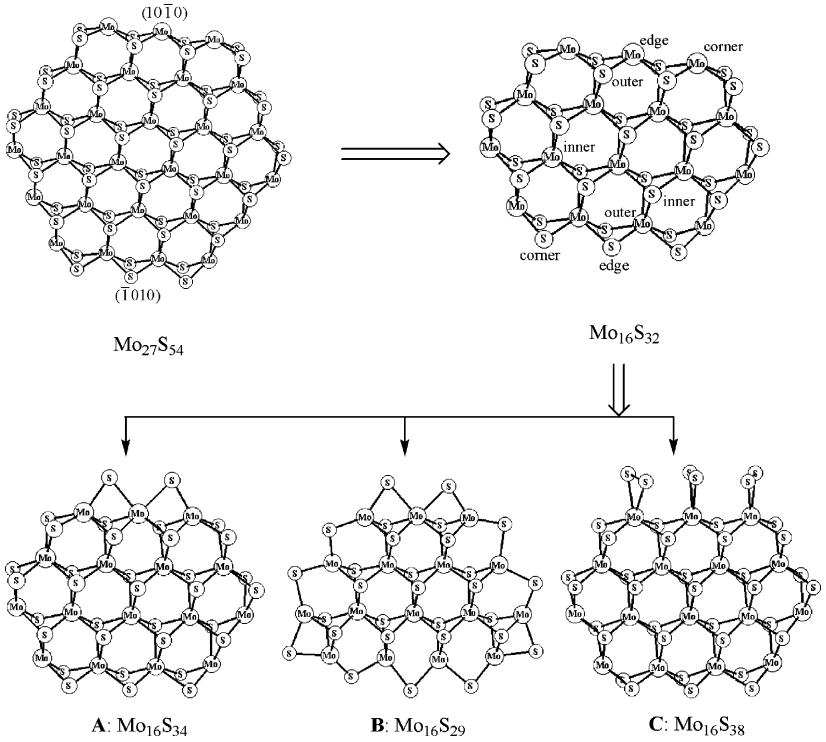

Figure 1. $Mo_{16}S_x$ ($x = 32, 34, 29, 38$) modes deduced from $Mo_{27}S_{54}$. $Mo_{16}S_{32}$: (10$\bar{1}$0) covered 0% with S, and ($\bar{1}$010) covered 100% with S. **A**: (10$\bar{1}$0) covered 50% with S, and ($\bar{1}$010) covered 100% with S. **B**: Both (10$\bar{1}$0) and ($\bar{1}$010) covered 50% with S. **C**: Both (10$\bar{1}$0) and ($\bar{1}$010) covered 100% with S.

phenomenon to the steric effect inhibiting tilted adsorbed COs. Recently, Koizumi et al.[14] performed in situ diffuse reflectance infrared Fourier transform studies of CO HYD on MoS_x, and they found that the peak near 2100 cm^{-1} detected at the beginning of the reaction disappeared immediately after the start of the reaction. This indicates that the adsorbed CO with a frequency at 2100 cm^{-1} is little involved in the HYD process. The coordinatedly unsaturated Mo atoms on reduced surfaces play the key roles for CO adsorption and activation. The more reduced the surface, the stronger the CO activation and adsorption.

In this article, we wish to report theoretical studies on CO adsorption on different active sites of four $Mo_{16}S_x$ ($x = 32, 34, 29, 38$) stoichiometric and nonstoichiometric clusters to model the changes of surface structure and composition. The C−O stretching frequencies were calculated and compared with available experimental and theoretical data. It is found that CO prefers adsorption on the coordinatively unsaturated (10$\bar{1}$0) surface, and there is no significant repulsive interaction between the end-on adsorbed CO probes at high coverage.

Models and Methods

1. Models. MoS_2 has a closely packed layered sandwich structure with each Mo atom coordinated by six sulfur atoms in a prismatic unit, and Mo atoms are in a plane situated between two sulfur planes.[15] It is found that small MoS_2 slabs are responsible for the catalytic activities of HYD.[16] As shown in Figure 1, there are two primary surfaces, (10$\bar{1}$0) and ($\bar{1}$010), on a MoS_2 slab, and the former may be of essential importance for the catalytic activity of CO HYD.[17,18] It has long been known that the active phase of HYD over MoS_x is highly dispersed MoS_x crystal in nanosizes with boundaries in all crystallographic directions. More recently, the scanning tunneling microscopy revealed a truncated hexagon form for MoS_2 cluster under excess hydrogen.[19] These boundaries indicate that using cluster models to describe the behaviors of MoS_2 is more reasonable than using periodic models. This is because the cluster models have an identifiable corner and side as suggested by Müller et al.[6] and Elst et al.,[7] while periodic models show only the edge site.

Li et al.[20] and Ma et al.[21] as well as Orita et al.[22] spotted the theoretic finite $Mo_{27}S_{54}$ cluster in Figure 1 as the best model for MoS_2 particles.[23] Later, Orita et al.[24] found that a simplified $Mo_{16}S_{32}$ (Figure 1) can also model effectively, on one hand, the adsorption of thiophene, which is by far bigger than CO and needs more active sites than CO adsorption, and on the other hand, reduce the computation costs considerably. On this basis, $Mo_{16}S_{32}$ can also represent the real highly dispersed MoS_2 particle with less cost. Furthermore, we compared several CO adsorption modes on both $Mo_{16}S_{32}$ and $Mo_{27}S_{54}$ clusters, and the results are in good consistence; for example, the adsorption energy (E_{ads}) of the bridge mode on $Mo_{27}S_{54}$ is −1.94 eV, while that on $Mo_{16}S_{32}$ is −1.93 eV. Thus, $Mo_{16}S_{32}$ is large enough to simulate the adsorption of CO on MoS_2. However, both $Mo_{27}S_{54}$ and $Mo_{16}S_{32}$ have (10$\bar{1}$0) without sulfur and ($\bar{1}$010) fully covered by sulfur (100%), respectively, and they do not represent the models for nonstoichiometric MoS_x cluster. On the basis of this and on the literature,[4] we constructed three clusters (**A**−**C**) to model the nonstoichiometric or defect MoS_x surfaces (Figure 1).

2. Methods. All calculations were done with the program package Dmol[25] in the Material Studio of Accelrys Inc. For structure optimizations and energy calculations, the density functional semi-core pseudopotential[26] was used for molybdenum, while the doubled numerical basis set with p- and d-polarization functions was used for all other elements. The gradient-corrected functional by Perdew and Wang (PW91[27]) was used, and real space cutoff of atomic orbital was set at 5.5 Å. The FINE standards for the tolerances of energy, gradient, displacement, and self-consistent field convergence criteria of 1×10^{-5} au, 2×10^{-3} au/Å, 5×10^{-3} Å, and 1×10^{-6} au,

respectively, were employed, and the MEDIUM quality mesh size of the program for the numerical integration was adopted. In our calculation, restricted spin polarization was used because the cluster $(MoS_2)_y$ with $y \geq 7$ favors the singlet state.[28] Indeed, we also searched the spin state for several adsorption conformations, and those results identified the singlet state as the ground state. Thus, using restricted spin polarization can enhance computational efficiency without loss of accuracy.

For the interaction between CO and surface, we used the adsorption energy as defined in eq 1, in which E(cluster) and E(CO) are the energies of the separated cluster and free CO, while $E(CO)_n$/cluster represents the energy of the adsorbed CO complex, and n is the number of the adsorbed CO molecules. On the basis of this equation, the more negative the adsorption energy, the stronger the adsorption.

$$E_{ads} = E((CO)_n/\text{cluster}) - [E(\text{cluster}) + nE(CO)] \quad (1)$$

To study the influence of the increased coverage, it is necessary to compare the difference (ΔE_{ads}) in adsorption energy between the higher coverage (E_{ads}, $n > 1$) and the sum of the single CO adsorption (ΣE_{ads}, $n = 1$). This is defined in eq 2.

$$(\Delta E_{ads}) = (E_{ads}, n > 1) - \Sigma(E_{ads}, n = 1) \quad (2)$$

The vibrational frequencies of the adsorbed CO were calculated by numerical differentiation of the force matrix. To reduce cost, we computed only the matrix corresponding to C and O. Travert et al.[5] found that the CO stretching mode is only very weakly coupled with the vibrations of the surface, so this approximation should not result in large systematic errors. After fitting the calculated and experimental CO stretching vibrations of free CO molecule, we got a scaling factor of 1.01, which is very close to that (1.02) of Travert et al.[5] All calculated frequencies are scaled by 1.01.

Results and Discussion

1. Clusters. According to the coordinating environments in Figure 1, all sulfur atoms in $Mo_{16}S_{32}$ can be classified into four groups; S_c, S_e, S_o, and S_i. All Mo atoms can be classified into Mo_c, Mo_e, Mo_o, and Mo_i. The subscripted letters, c, e, o, and i, mean the *c*orner, *e*dge, *o*uter, and *i*nner positions of atoms, respectively. In addition to $Mo_{16}S_{32}$, the three non-stoichiometric clusters (**A**−**C**) of defect $(\bar{1}010)$ are employed to model the changes and reconstruction of the surface under real reaction condition, and the non-stoichiometric S on $(\bar{1}010)$ is unanimously noted as S_n.

As shown in Figure 1, $Mo_{c/IV}$ and $Mo_{e/IV}$ in $Mo_{16}S_{32}$ and $Mo_{c/IV}$ and $Mo_{o/IV}$ in cluster **B** have 2-fold coordinatively unsaturated sites (CUS), while $Mo_{c/V}$ in cluster **A** has a 1-fold CUS (Roman numbers mean the coordination number of each atom). They should be mainly responsible for CO adsorption. In contrast, cluster **C** does not have any CUS, so CO adsorption on this cluster should be very weak or unlikely. Since $(\bar{1}010)$ of $Mo_{16}S_{32}$, clusters **A** and **C**, is identical, we only calculated CO adsorption on $Mo_{16}S_{32}$'s $(\bar{1}010)$ and transferred the results to clusters **A** and **C**.

2. CO Adsorption on $Mo_{16}S_{32}$. Although according to the literature,[4] $(10\bar{1}0)$ covered with 0% S and $(\bar{1}010)$ covered with 100% S will not present simultaneously, the investigation of CO adsorption on $Mo_{16}S_{32}$ still makes sense. According to previous work,[4,5] these two surfaces take part in chemical reaction independently, and the results about this cluster can be transferred to other clusters having 0% S-covering $(10\bar{1}0)$ or 100% S-covering $(\bar{1}010)$. Thus, study of CO adsorption on each surface is necessary. The optimized adsorption forms for one, two, and six CO molecules are shown in Figure 2, and the computed structural parameters and E_{ads} values are given in Table 1.

i. One CO Adsorption on $(10\bar{1}0)$. As given in Table 1, all three forms (**1**−**3**) on $(10\bar{1}0)$ are strongly exothermic, indicating the high activity for CO adsorption. In contrast to Mo in bulky MoS_2 phase with six S coordination, the Mo in the reduced $(10\bar{1}0)$ surface in our model is only coordinated by four S atoms. These Mo atoms are 2-fold unsaturated, and they need more ligands to saturate them. Both side and bridge adsorptions (**2** and **3**) are stronger than the corner model (**1**), as indicated by their adsorption energies (−1.94 and −1.93 eV vs −1.80 eV). Despite the bridged CO, **3** has nearly the same adsorption energy as **2**.

In **1** and **2**, the Mo_c−C and Mo_e−C distances are 2.037 and 2.027 Å. In **3**, the Mo_c−C and Mo_e−C distances are 1.991 and 2.030 Å, respectively, and the Mo_e−O distance is 2.331 Å. In addition, the degree of the CO activation is reflected by the corresponding C−O bond lengths. As shown in Figure 2, the CO bond lengths of **1** and **2** are 1.160 and 1.164 Å, respectively, and they are shorter than that (1.229 Å) of **3**. The changes of the bond lengths are in line with the computed CO stretching frequencies (Table 1); for example, the largest shift is found for the bridged mode (**3**), and the corner and side adsorption modes (**1** and **2**, respectively) have lower shifts. On the basis of the orientation of adsorbed CO and the calculated adsorption energy, the bridge adsorbed CO is more activated.

ii. One CO Adsorption on $(\bar{1}010)$. There are two forms (**4** and **5**) on $(\bar{1}010)$, and the computed adsorption energies and bond lengths are given in Table 1. Among them, the top form (**4**) is more favored than the one with sulfur bridge (**5**), as indicated by the calculated adsorption energies (−0.95 vs −0.51 eV). The Mo−C distances of **4** are 2.079 Å, respectively. As compared with those of S-bare $(10\bar{1}0)$, fully S-covering $(\bar{1}010)$ shows very weak affinity to adsorb CO and is not competitive at lower coverage. This large difference in adsorption energy (up to 1 eV) can be ascribed to the difference of the Mo environment. For example, the Mo centers to CO in **1**−**3** with four connecting S atoms are 2-fold unsaturated, while that in **4** with six surrounding sulfurs are saturated. On the basis of these results, we focus on the higher coverage only on $(10\bar{1}0)$ in the following calculation about $Mo_{16}S_{32}$.

iii. Two CO Adsorption on $(10\bar{1}10)$. As shown in Figure 1, there are more than one CUS on $(10\bar{1}0)$. This provides the opportunity to study the influence of two adsorbed CO probes on near sites and the adsorption ability of each CUS. On $(10\bar{1}0)$, six adsorption forms were obtained, and they are noted as corner/corner (**6**), side/side (**7**), corner/bridge (a) (**8**), corner/bridge (b) (**9**), corner/corner′ (**10**), and corner/side (**11**) in Figure 2.

As given in Table 1, all adsorption forms (**6**−**11**) have exothermic adsorption energies, and this indicates that it is possible for the S-bare $(10\bar{1}0)$ to adsorb one additional CO probe molecule, despite the geminal CO adsorption in **6** and **7**. Attempts to get the doubly bridged CO adsorption failed, and optimization led to the corner/bridge (a) (**8**) or the corner/bridge (b) (**9**). In addition, it also is not possible to get the adsorption form with one side CO and bridged side CO, and optimization led to corner/side (**11**). The most stable adsorption forms are **8** and **11**, followed by **10**, while **6**, **7** and **9** are less stable, and the largest difference in adsorption energy is only 0.24 eV.

In addition to the structures, it is also interesting to compare their adsorption energies with that of the mono adsorption. As given in Table 1, the adsorption energies for **6**, **8**, **10**, and **11**

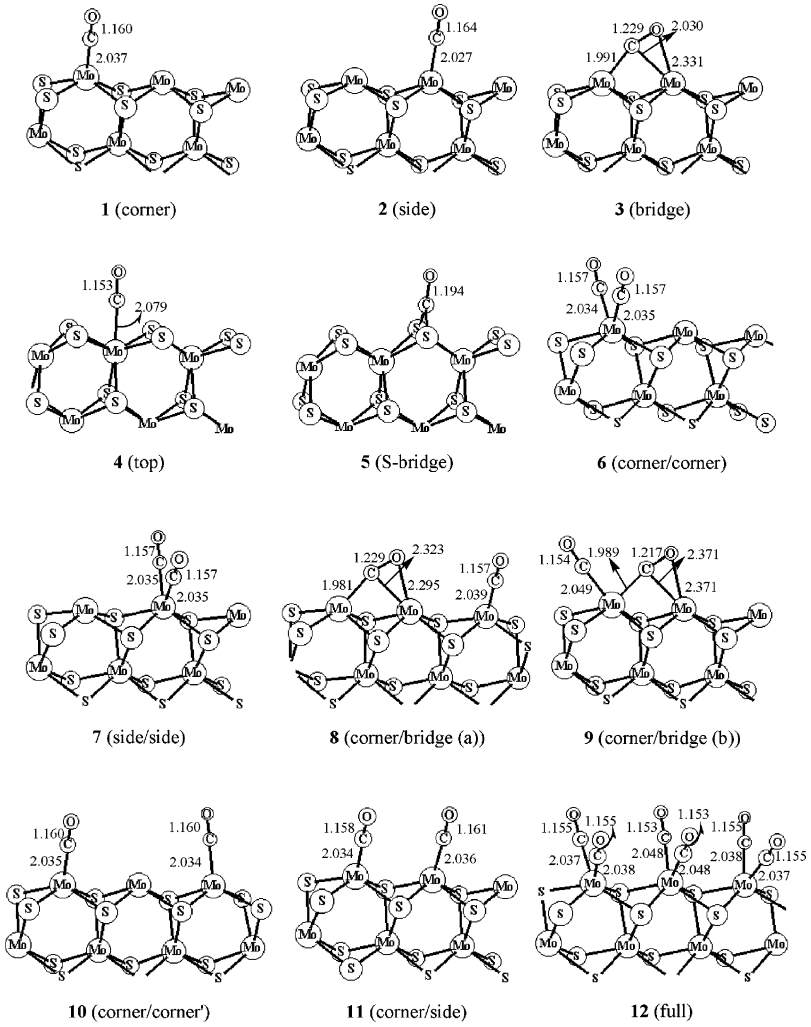

Figure 2. Adsorption structures on cluster $Mo_{16}S_{32}$ with one (**1**−**5**), two (**6**−**11**), and six (**12**) adsorbed CO probes.

TABLE 1: Computed Adsorption Energies (E_{ads}, eV) and Their Differences to One CO Adsorption (ΔE_{ads}, eV), as Well as CO Vibrational Frequency (cm^{-1}) and the Selected Bond Lengths (R, Å)[a]

mode		E_{ads} (ΔE_{ads})[b]	υ (CO)	R_{Mo-C}	R_{C-O}
		One CO Adsorption			
1 (corner)		−1.80	1992	2.037	1.160
2 (side)		−1.94	1970	2.027	1.164
3 (bridge)		−1.93	1545	1.991	1.229
4 (top)		−0.95	2053	2.079	1.153
5 (S-bridge)		−0.51	1781		1.194
		Two CO Adsorption			
6 (corner/corner)		−3.56 (+0.04)		2.035/2.035	1.157/1.157
7 (side/side)		−3.50 (+0.38)		2.035/2.035	1.157/1.157
8 (corner/bridge (a))		−3.68 (+0.04)		2.039/1.981	1.157/1.229
9 (corner/bridge (b))		−3.44 (+0.28)		2.049/1.989	1.154/1.217
10 (corner/corner′)		−3.60 (0.00)		2.034/2.035	1.160/1.160
11 (corner/side)		−3.68 (+0.08)		2.034/2.036	1.158/1.161
		Six CO Adsorption			
12 (full)	corner site	−10.45 (+0.63)	2049, 2039, 2037, 2035	2.037/2.038	1.155
	side site		2016, 2028, 2005[c], 2008[d]	2.048	1.153

[a] The frequency and bond length of free CO are 2143 cm^{-1} and 1.140 Å. [b] According to eq 2. [c] Coupled stretching frequencies. [d] Identifiable stretching frequencies.

are additive as compared with their corresponding one CO adsorption, while those of **7** and **9** are slightly smaller. This indicates that the two adsorbed CO probes are "isolated" in **6**, **8**, **10**, and **11**, while somewhat repulsive interaction occurs in **7** and **9**. Obviously, the result, that the bridge CO is sensitive to the high coverage, is consistent with the experimental results by Jaworowski et al.[13]

It is interesting to note the different adsorption energies of **7** and **8** with geminal COs as compared with their one CO adsorption (+0.04 vs +0.38 eV). This difference can be ascribed to the local environment of the CUS. As shown in Figure 3, at the corner position of $Mo_{16}S_{32}$, for example, Mo has four coordinating sulfurs, and two of them coordinate with two Mo centers and the other two with three Mo centers, and the Mo−S

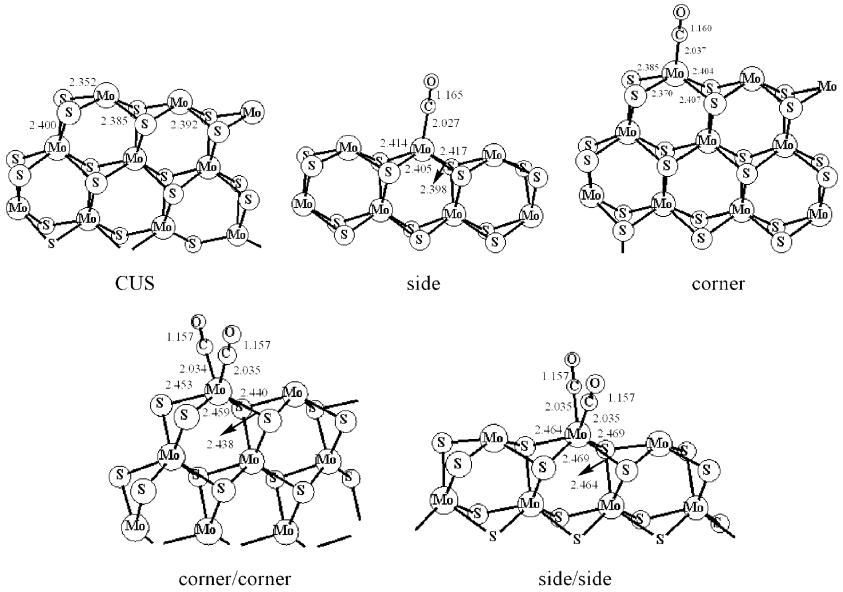

Figure 3. Local structural differences of the corner and side CUS, and their one and two CO adsorption forms of $Mo_{16}S_{32}$.

distance of the former case (2.352 Å) is shorter than that of the latter case (2.385 Å). At the side position, all four sulfurs coordinate with three Mo centers, with the Mo−S distances in the range of 2.385−2.392 Å. The longest Mo−S distance is found at the top position by 2.400 Å. This indicates that CUS at the corner can relax more than at the side.

With CO adsorption, the local Mo−S distances become longer, and the magnitude of the elongation depends on the adsorbed CO numbers; for example, the Mo−S distances with two geminal adsorbed COs are longer than those with one CO. We note that the Mo−C distances in one corner (**1**) and two corners (**6**) are very close (2.037 vs 2.035 Å), while those in two side forms (**7**) are longer than in one side form (**2**) (2.035 vs 2.027 Å), respectively. This reflects the additivity of the adsorption energy in corner coordination and the difference in side coordination.

iv. Adsorption under Higher Coverage on (10$\bar{1}$0). Since each CUS on (10$\bar{1}$0) can adsorb two COs to saturate the coordination sphere in high adsorption energies, the full adsorption of all CUS under the appropriated concentration of CO should be possible. Therefore, we have considered the full coordination on corner and side with totally six CO probes (**12**), as shown in Figure 2. Indeed, the calculated adsorption energy of −10.45 eV is very high (Table 1). It is interesting to note that this adsorption energy has still the additivity (−10.62 eV) as compared with those of the two corner/corner and one side/side adsorptions in Figure 2 and Table 1, and full adsorption has only minor effect on energy. On this basis, one might consider that the six adsorbed CO probe molecules are "isolated" and do not interact with each other. Thus, the control of selective adsorption can only be made by the control of CO concentration.

Frequency calculations were performed on **12**, which provide each kind of adsorbed CO probe molecules under certain coverage. According to the literature,[5,6,8,9] there is a band at 2070−2060 cm^{-1} with a tail at 2000−2020 cm^{-1} for CO/MoS_2. Our results show that all CO frequencies are among this band. Because of the overlap of the equally adsorbed CO probes, it is hard to identify the stretching frequency of individual CO experimentally.

3. CO Adsorption on Non-Stoichiometric Clusters. Apart from $Mo_{16}S_{32}$, three non-stoichiometric clusters (**A**−**C**) of defect (10$\bar{1}$0) are employed to model the CO adsorption on the changed surface composition and structure under real reaction condition. The optimized adsorption forms for one CO, two CO, and six CO molecules are shown in Figure 4, and the computed structural parameters and E_{ads} values are given in Table 2.

i. One CO Adsorption Cluster A ($Mo_{16}S_{34}$). As shown in Figure 4, cluster **A** can adsorb CO at three different sites, that is, at the corner (**13**), at the side (**14**), and bridged CO (**15**). As given in Table 2, CO adsorption in **13** is stronger than that in **14**, as indicated by their E_{ads} values (−1.06 and −0.53 eV) and the Mo−C distances (2.072 and 2.138 Å). This is in line with the different coordinating sites at Mo. In contrast, the bridged mode (**15**) is endothermic, which is in contrast to that of one CO adsorption on $Mo_{16}S_{32}$, in which both bridged and end-on CO adsorptions are possible. This should be due to the formation of the three-membered ring and the raised strain energy. Thus, this unrealistic mode has been ruled out in the following investigation.

Along with the E_{ads} values, the C−O bond lengths reflect the degree of CO activation. As shown in Figure 4, the C−O bond lengths of **13** and **14** are 1.153 and 1.145 Å, respectively, and are longer than that (1.140 Å) of free CO. In addition, the changes of C−O distances are in line with the calculated frequencies (Table 2). Both 2080 and 2045 cm^{-1} peaks for the side and corner CO are in the characteristic range of 2070 cm^{-1} centered broad band of CO adsorbed on MoS_2. Compared with the corresponding modes of one CO adsorptions on the stoichiometric $Mo_{16}S_{32}$ (−1.80 and −1.94 eV), the adsorption and activation of CO in **13** and **14** are by far weaker, and this is in accordance with the general theory that the more reduced the surface, the stronger the adsorption and activation of the adsorbed COs.

ii. Two CO Adsorption. As shown in Figure 4, cluster **A** can adsorb two CO molecules at four different sites, that is, at geminal corner/corner (**16**), at geminal side/side (**17**), at corner/side (**18**), and at two separated corner/corner′ (**19**). As given in Table 2, all adsorption are exothermic, indicating the thermodynamic possibility for the second CO adsorption at the 50% S-covered (10$\bar{1}$0) surface, and **12** is the most stable mode with end-on CO coordination. This is in contrast to those of double CO adsorption on $Mo_{16}S_{32}$, in which combined bridged/end-on and end-on/end-on CO adsorptions are possible.

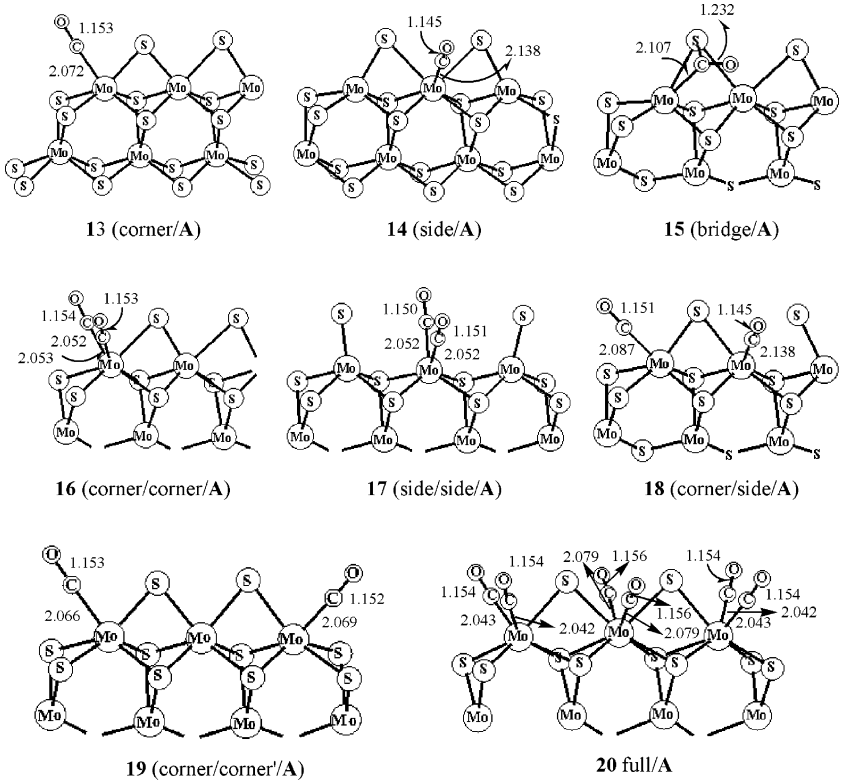

13 (corner/**A**) **14** (side/**A**) **15** (bridge/**A**)

16 (corner/corner/**A**) **17** (side/side/**A**) **18** (corner/side/**A**)

19 (corner/corner′/**A**) **20** full/**A**

Figure 4. Adsorption structures on cluster $Mo_{16}S_{34}$ (**A**) with one (**13**−**15**), two (**16**−**19**), and six (**20**) adsorbed CO probes

TABLE 2: Computed Adsorption Energies (E_{ads}, eV) and Their Differences to One CO Adsorption (ΔE_{ads}, eV), as Well as CO Vibrational Frequency (cm^{-1}) and the Selected Bond Lengths (R, Å) on Cluster A

mode	E_{ads} (ΔE_{ads})[a]	R_{Mo-C}	R_{C-O}	υ (CO)
		One CO Adsorption		
13 (corner/**A**)	−1.06	2.072	1.153	2045
14 (side/**A**)	−0.53	2.138	1.145	2080
15 (bridge/**A**)	+0.47	2.107	1.232	1571
		Two CO Adsorption		
16 (corner/corner/**A**)	−1.99 (0.08)	2.053/2.052	1.153/1.154	
17 (side/side/**A**)	−2.09 (−1.03)	2.052/2.052	1.150/1.151	
18 (corner/side/**A**)	−1.57 (0.02)	2.087/2.138	1.151/1.145	
19 (corner/corner′/**A**)	−2.23 (−0.10)	2.066/2.069	1.153/1.152	
		Six CO Adsorption		
20 (full/**A**)	−4.26 (1.05)	2.042/2.043	1.154	2057/2055[b]
		2.079	1.156	2007/2003[c]

[a] Difference to the sum of one CO adsorption (eq 2). [b] R_{Mo-C}, R_{C-O}, and frequencies of corner CO. [c] R_{Mo-C}, R_{C-O}, and frequencies of side CO.

The E_{ads} values of **16**, **18**, and **19** show the approximated additivity. However, the most intriguing case is the geminal side/side adsorption (**17**), in which the two sulfur bridges are converted into two terminal sulfurs and the Mo_e center has totally changed to a stable six-coordinated one, like the bulky Mo, and the E_{ads} value of −2.09 eV is much more negative than the sum of two side adsorption in **14** (−0.53 eV).

iii. Adsorption at Higher Coverage. Considering the real working condition of CO HYD, it is necessary to investigate CO adsorption on MoS_2 catalyst under high CO concentration. On the basis of previous calculations, we have considered the full coordination on both corner and side with totally six CO probes (**20**), as shown in Figure 4. Its E_{ads} value is −4.26 eV, while its ΔE_{ads} value is positive by 1.05 eV, and this indicates the thermodynamically unfavored process. This change can be ascribed to the repulsion between the side CO and the S_n. Frequency calculations provided four characteristic frequencies of 2057 and 2055 for the corner CO and 2007 and 2003 cm^{-1} for the side CO. Considering the full adsorption at corner, two geminal CO side adsorption at high concentration will be unlikely.

iv. A Specific Discussion about Frequencies. Thus far, most of the calculated frequencies are lower than the experimental band center at 2070 cm^{-1}, except 2080 cm^{-1} in **14**, which is very close to the band center. However, there is only one side site in cluster **A**, and the frequency at 2080 cm^{-1} cannot represent the characteristic IR spectra from experiment.

Nevertheless, one should keep in mind that the predominant sizes of highly dispersed MoS_2 catalysts within 10−30 Å[21,29] should have a much larger number of Mo_e centers for one CO side adsorption as in **14**. Considering the real size MoS_2 has a hexagonal shape with six corners, the Mo_e/Mo_c ratio should be $3m/6$, where m is the number of Mo_e on each $(10\bar{1}0)$. This considerably increases the probability of one CO adsorption at Mo_e with the enlarged $(10\bar{1}0)$. On the other hand, most Mo_e centers in real size are adjacent to each other, and their bridged

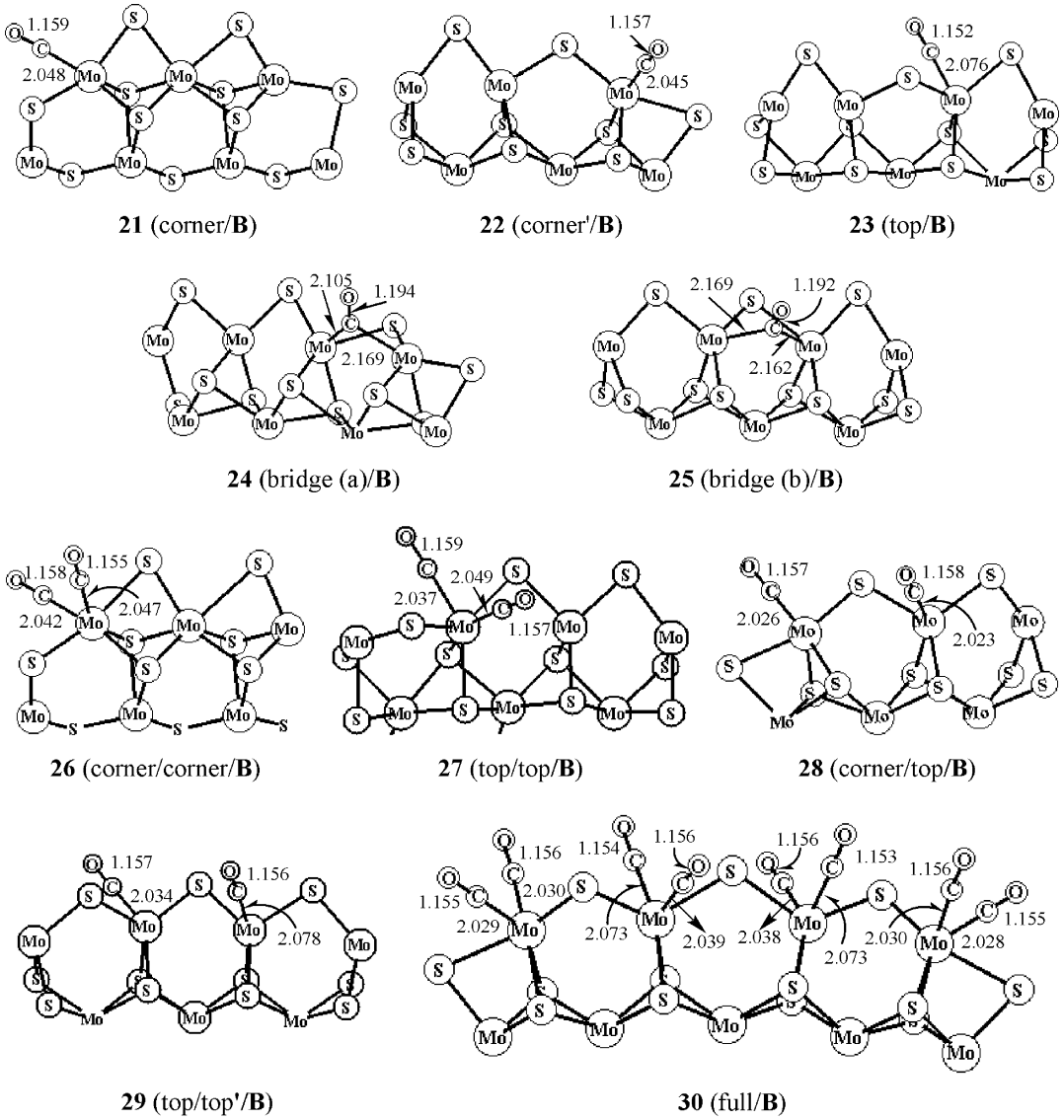

Figure 5. Adsorption structures on cluster $Mo_{16}S_{29}$ (**B**) with one (**21**−**25**), two (**26**−**29**), and eight (**30**) adsorbed CO probes

Mo_e-S_n bonds should not be broken as easily as in **17**; therefore, they will be unlikely to adsorb one additional CO.

On this basis, the number of one side CO adsorption (like **14**) in real size MoS_2 should be by far larger than that of the corner one. Consequently, the weighted IR band center should blue-shift to the frequency of one side CO, as observed experimentally.

4. CO Adsorption on Cluster B ($Mo_{16}S_{29}$). As shown in Figure 1, cluster **B** has 2-fold unsaturated Mo sites for CO adsorption on $(\bar{1}010)$. Since the local structure of Mo_e of cluster **B** is identical to that of cluster **A**, any side adsorption mode will be neglected.

i. One CO Adsorption. On the basis of cluster **B**, five mono CO adsorption modes were obtained. The optimized structures are illustrated in Figure 5, and the calculated adsorption energies and bond lengths are listed in Table 3. Structures **21** and **22** have corner adsorption, while **23** has top mode. Structures **24** and **25** have adsorbed CO bridging two Mo centers. On the basis of the calculated E_{ads} value, the most stable modes are **21** and **22**, while **23**−**25** are less stable (−1.35 and −1.28 vs −1.10, −0.88, and −0.61 eV, respectively). In addition, **22** is the precursor for further CO adsorption at top to form the full mode. Energetically, the formation of bridged modes is not favored on one hand, and on the other hand experimental IR does not support their stretching frequencies. Therefore, these bridged CO probes should not exist under real conditions, and they are ruled out in the following part.

As compared to **13**, the adsorption and activation of CO in **21** are stronger, as indicated by the $C-Mo_c$ and C−O distances, because of the difference in the number of CUS at the Mo_c center. For the same reason, the tilted bridge mode, corresponding to **15**, could not be located and was optimized to **21** directly without any barrier. However, the adsorption and activation in **21** are still weaker than in **1**, as indicated by the E_{ads} values (−1.35 vs −1.80 eV). Although both Mo_c's are 2-fold CUS, the Mo_c in $Mo_{16}S_{32}$ cluster has higher activity.

ii. Two CO Adsorption. Considering only corner and top sites, four two CO adsorption modes are obtained. The optimized structures are illustrated in Figure 5, and the calculated E_{ads} values and bond lengths are listed in Table 3. All E_{ads} values in Table 3 are negative, indicating the potential for additional CO adsorption. On the basis of adsorption energies, **26** is the most stable mode for the one geminal corner/corner adsorption, followed by **28** (corner/top) and **29** (top/top′ with trans angular CO molecules). As expected, the E_{ads} values of **26**, **28**, and **29** show the additivity, while that of **27** (geminal top/top) is smaller

TABLE 3: Computed Adsorption Energies (E_{ads}, eV) and Their Differences to One CO Adsorption (ΔE_{ads}, eV), as Well as CO Vibrational Frequency (cm^{-1}) and the Selected Bond Lengths (R, Å) Cluster B

mode	E_{ads} (ΔE_{ads})[a]	R_{Mo-C}	R_{C-O}	υ (CO)
		One CO Adsorption		
21 (corner/**B**)	−1.35	2.048	1.159	1965
22 (corner′/**B**)	−1.28	2.045	1.157	1995
23 (top/**B**)	−1.10	2.076	1.152	2023
24 (bridge (a)/**B**)	−0.88	2.105/2.169	1.194	1787
25 (bridge (b)/**B**)	−0.61	2.161/2.169	1.192	1789
		Two CO Adsorption		
26 (corner/corner/**B**)	−2.80 (−0.11)	2.047/2.042	1.155/1.158	
27 (top/top/**B**)	−1.53 (0.67)	2.049/2.073	1.157/1.159	
28 (corner/top/**B**)	−2.31 (0.08)	2.026/2.023	1.157/1.158	
29 (top/top′/**B**)	−2.05 (0.16)	2.034/2.078	1.157/1.156	
		Eight CO Adsorption		
30 (full/**B**)	−8.53 (0.99)	2.030	1.156	2065/2048
		2.029	1.155	2042/2042
		2.028		2042/2016[b]
		2.073	1.156	2034/2020
		2.039	1.154	2000/1982
		2.038	1.153	2043/2027[c]

[a] Difference to the sum of one CO adsorption (eq 2) [b] R_{Mo-C}, R_{C-O} of corner CO, and unidentifiable frequencies. [c] R_{Mo-C}, R_{C-O} of top CO, and identifiable frequencies.

than the expected value ($\Delta E_{ads} = 0.67$ eV), and this can be attributed to the repulsion of the geminal CO molecules and the S_o.

iii. Adsorption at Higher Coverage. On the basis of the most favored adsorption modes discussed above, we have considered the full CO adsorption with two geminal corner/corner and two geminal top/top by totally eight CO probes (**30**), as shown in Figure 5. The large E_{ads} value of −8.53 eV shows the rough additivity compared to **26** with geminal corner/corner and **27** geminal top/top coordination (−8.66 eV), but it is slightly lower than that of the corresponding single CO adsorptions (−9.52 eV). This indicates that **30** can exist at high CO concentration. In addition, all calculated frequencies are within the range of the characteristic band of experimental IR. Unlike those of cluster **A**, C−O stretching vibrations are highly coupled and hardly identifiable.

5. CO Adsorption on Cluster C ($Mo_{16}S_{38}$). Several conformations including one CO probe on $(10\bar{1}0)$ were subjected to optimization, but in all final structures, the CO was separated from the original Mo site, which indicates that no adsorption is possible on this surface. It is obvious that the coordination of these surface Mo centers is identical to that of the bulky Mo, which is inert for CO adsorption. Therefore, neither structural nor energetic data are available on cluster **C**.

6. Comparison of Frequencies with Results from Periodic Models. Travert et al.[5] used periodic models to perform a systematic study of CO adsorption on MoS_2, and they tried assigning calculated frequencies to experimental spectra. On their nonnaked $(10\bar{1}0)$, covered by bridged S, one end-on CO adsorption mode, like **14**, was obtained, and the calculated C−O stretching frequency is 2080 cm^{-1}, which is exactly identical to our result for **14**. On the other hand, their calculated frequency of end-on CO on fully S-covering $(\bar{1}010)$, corresponding to **4**, is 2040 cm^{-1}, which is quite close to our 2053 cm^{-1} (under high CO coverage, lowered to 2048 cm^{-1}) result. These two points can benchmark that our model is big enough, for such little surfaces can present results close to those from periodic models. It might argue that the fully S-covering $(\bar{1}010)$ only exists under a high H_2S/H_2 ratio, under which MoS_2 cluster is in triangle shape,[19] and then the fully S-covering $(\bar{1}010)$ of a hexagon cluster is an unreasonable model. However, we should notice that first, the Mo_o, the main adsorption site on $(\bar{1}010)$, is not situated on the corner, which is the main difference between hexagon and triangle. Second, **4**'s frequency result agrees perfectly with that from an infinite periodic model. Thus, although our fully S-covering $(\bar{1}010)$ is on a hexagon cluster, its results can still represent CO adsorption on this surface. As to the half S-covering $(\bar{1}010)$, Travert et al. got 1965−2000 cm^{-1} frequencies for the mode corresponding to **23** under a range of coverage, while we got similar results of 1982−2023 cm^{-1}. Generally speaking, our results of noncorner adsorptions are in good consistency with their results, and furthermore, we can provide corner adsorptions, which is not the case from periodic model.

7. Reactivity of Adsorbed CO. According to Muramatsu et al.,[30] the dissociated CO favors the chain propagation, and then the synthesis of the higher hydrocarbons and alcohols, whereas the undissociated CO favors the synthesis of the C_1 product. According to Pavão et al.,[3] the bridged CO is a typically tilted state, which interacts with two adjacent metal atoms. As to the S-bare $(10\bar{1}0)$, from the C−O bond activation (Figure 2), the bridged CO seems to be the most activated and has the tendency to dissociate. Its unusually low C−O stretching frequency of 1545 cm^{-1} is consistent with the characteristic frequencies of tilted CO adsorbed on transition metal surfaces. Thereby, the bridged CO can be considered as the precursor for the synthesis of higher hydrocarbons and alcohols.

However, the bridged CO has the same adsorption energy as the side mode (Table 1), and both modes are equally favored and populated under the equilibrium. Therefore, it is not possible to control the adsorption mode at low CO concentration. At higher coverage, there are only corner and side modes and no bridged CO is found. As to other surfaces, no bridged CO is favored at all. Without bridged CO, chain propagation would hardly happen, and this is probably why the MoS_2 phase has low selectivity toward the production of higher hydrocarbons and alcohols. Indeed, Koizumi et al. performed a CO HYD process over MoS_2/Al_2O_3 catalyst, and the main products are CO_2 and CH_4.[14] In addition, Li et al.[31] found that the main product by CO HYD over K/MoS_2 is CH_3OH.

In contrast to the MoS_2 phase, iron-based catalysts used in the Fischer−Tropsch synthesis produce long-chain *n*-alkanes and *n*-alkenes as the major product.[32] Recent theoretical analysis[33] showed that the adsorbed CO molecules over the iron

carbide surfaces (Fe_5C_2) prefer the titled states and interact with two (2-fold), three (3-fold), or four (4-fold) surface irons, and these interactions lead to the formation of C−C bonds. The calculated adsorption energies at low coverage on Fe_5C_2 (−2.1 to −2.3 eV) are higher than those on MoS_2 (<2 eV). This indicates that Fe_5C_2 can activate CO more effectively than MoS_2.

Summary and Conclusion

DFT calculations are carried out to study CO adsorption at the CUS of four $Mo_{16}S_x$ (x = 32, 34, 29, 36) catalysts. The goal of this investigation is to understand CO adsorption on the changes of surface structure and composition. On the basis of the calculated CO adsorption energies of clusters **A** and **B** on both $(10\bar{1}0)$ and $(\bar{1}010)$ surfaces, we find that the corner sites are the most favored and are the active center for one and two geminal CO molecules and that other sites are not competitive at low CO concentration. At very high CO concentration, adsorption at edge and top sites becomes possible. In all cases, end-on CO coordination is predominant, while titled or bridged CO coordination is unlikely. This is why that CO HYD process catalyzed by these clusters can only yield C_1 products, and no higher alcohols or hydrocarbons have been found. It is very informative to compare the adsorption on the stoichiometric and nonstoichiometric surfaces. For one and two CO adsorptions, stoichiometric ($Mo_{16}S_{32}$) surfaces can have both end-on and bridged CO molecules, while only end-on CO molecules on nonstoichiometric surfaces are possible. At high CO concentration or high coverage, however, both stoichiometric and nonstoichiometric surfaces prefer only end-on CO adsorption.

The calculated CO stretching frequencies (2000−2080 cm^{-1}) are in very good agreement with the characteristic band observed experimentally (a broad band centered at 2070 cm^{-1} with a tail extent to 2000 cm^{-1}). Generally, this band, mainly responsible for the HYD process, is attributed to the adsorbed CO probes on 4- and 5-fold coordinated Mo centers. However, adsorbed CO on 5- or even 6-fold coordinated Mo center provides frequencies in this band as well. Considering the catalyst in real size and hexagonal form, the number of edge Mo is much higher than that of corner. This raises the probability of side coordination and the blue-shift of CO frequencies.

Acknowledgment. We thank for financial support the Key Project of Chinese Academy of Sciences and the 863 Project of Ministry of Science and Technology of China (2001AA523010 and KGC X1-SW-02), the Natural Science Foundation of Shanxi Province, China (20031022), and the Natural Science Foundation of China (20473111 and 20590360).

References and Notes

(1) Fukase, S.; Akashah, S. *Hydrocarbon Asia* **2004**, (Technology, Catalyst Suppl.-Part 1), 24.

(2) Sung, S.; Hoffmann, R. *J. Am. Chem. Soc.* **1985**, *107*, 578.

(3) Pavão, A. C.; Guimarães, T. C. F.; Lie, S. K.; Taft, A. A.; Lester, W. A., Jr. *J. Mol. Struct. (THEOCHEM)* **1999**, *458*, 99.

(4) (a) Raybaud, P.; Hafner, J.; Kresse, G.; Kasztelan, S.; Toulhoat, H. *J. Catal*. **2000**, *189*, 129. (b) Cristol, S.; Paul, J. F.; Payen, E.; Bougeard, D.; Hutschka, F. *J. Phys. Chem. B* **2000**, *104*, 11220. (c) Sun, M.; Adjaye, J.; Nelson, A. E. *Appl. Catal. A* **2004**, *263*, 131.

(5) Travert, A.; Dujardin, C.; Maugé, F.; Cristol, S.; Paul, J. F.; Payen, E.; Bougeard, D. *Catal. Today* **2001**, *70*, 255.

(6) Müller, B.; van Langeveld, A. D.; Moulijn, J. A.; Knözinger, H. *J. Phys. Chem.* **1993**, *97*, 9028.

(7) Elst, L. P. A. F.; Eijsbouts, S.; van Langeveld, A. D.; Moulijn, J. A. *J. Catal*. **2000**, *196*, 95.

(8) Peri, J. B. *J. Phys. Chem.* **1982**, *86*, 1615.

(9) (a) Maugé, F.; Lavalley, J. C. *J. Catal.* **1992**, *137*, 69. (b) Bachelier, J.; Tilliette, M. j.; Cornac, M.; Duchet, J. C.; Lavalley, J. C.; Cornet, D. *Bull. Soc. Chim. Belg.* **1984**, *93*, 743.

(10) Maugé, F.; Lamotte, J.; Nesterenko, N. S.; Manoilova, O.; Tsyganenko, A. A. *Catal. Today* **2001**, *70*, 271.

(11) Tsyganenko, A. A.; Can, F.; Travert, A.; Maugé, F. *Appl. Catal., A* **2004**, *268* 189.

(12) Iranmahboob, J.; Gardner, S. D.; Toghiani, H.; Hill, D. O. *J. Colloid Interface Sci.* **2004**, *270*, 123.

(13) Jaworowski, A. J.; Smedh, M.; Borg, M.; Sandell, A.; Beutler, A.; Sorensen, S. L.; Lundgren, E.; Andersen, J. N. *Surf. Sci.* **2001**, *492*, 185.

(14) Koizumi, N.; Bian, G.; Murai, K.; Ozaki, T.; Yamada, M. *J. Mol. Catal. A: Chem.* **2004**, *207*, 171.

(15) Wyckoff, R. W. G. *Crystal Structure*, 2nd ed.; John Wiley & Sons: New York, 1964; Vol.1, pp 280−281.

(16) (a) Delmon, B. In *Catalysts in Petroleum Refining-1989*; Trimm, D. L., Akashah, S., Absi-Halabi, M., Bishara, A., Eds.; Elsevier: Amsterdam, 1990; pp 1−40. (b) Delmon, B.; Froment, G. F. *Catal. Rev.−Sci. Eng.* **1996**, *38*, 69. (c) Topsøe, H.; Clausen, B. S.; Franklin, F. E.; Massoth, E. In *Science and Technology in Catalysis: Hydrotreating Catalysis*; Anderson, J. R., Boudart, M. Eds.; Springer: Berlin, 1996; Vol. 11. (d) Startsev, A. N. *Catal. Rev.−Sci. Eng.* **1995**, *37*, 353.

(17) (a) Kasztelan, S.; Jalowiecki, J.; Wambeke, A.; Bonnelle, J.; Bonnelle, J. P. *Bull. Soc. Chim. Belg.* **1987**, *96*, 1003. (b) Kasztelan, S.; Toulhoat, H.; Grimblot, J.; Bonnelle, J. P. *Appl. Catal.* **1984**, *13*, 127. (c) Wambeke, A.; Jalowiecki, L.; Kasztelan, S.; Grimblot, J.; Bonnelle, J. P. *J. Catal.* **1988**, *109*, 320. (d) Kasztelan, S. C. R. *Acad. Sci., Paris, Ser. II* **1988**, *307*, 727. (e) Toulhoat, H.; Kasztelan, S. In *Proc. 9th Int. Congr. Catal.*; Phillips, M. J., Ternan, M., Eds.; Chem. Inst. Canada: Ottawa, Canada, 1988; Vol. 7, p 152. (f) Kalthod, D. G.; Weller, S. W. *J. Catal.* **1985**, *95*, 455. (g) Tanaka, K.-I.; Okuhar, T. *J. Catal.* **1982**, *78*, 155. (h) Ratnasamy, P.; Sivasanker, S. *Catal. Rev.−Sci. Eng.* **1980**, *22*, 401. (i) Kasztelan, S.; Toulhoat, H.; Grimbolt, J.; Bonnelle, J. P. *Bull. Soc. Chim. Belg.* **1984**, *93*, 807.

(18) Inoue, Y.; Uragami, Y.; Takahashi, Y.; Eijsbouts, S. In *Science and Technology in Catalysis*, Proceedings of the third Tokyo Conference on Advanced Catalytic Science and Technology, Tokyo, Japan, July 19−24, 1998; Hattori, H., Otsuka, K., Eds.; Kodansha; Tokyo, 1998; p 415.

(19) Lauritsen, J. V.; Bollinger, M. V.; Lægsgaard, E.; Jacobsen, K. W.; Nørskov, J. K.; Clausen, B. S.; Topsøe, H.; Besenbacher, F. *J. Catal.* **2004**, *221*, 510.

(20) Li, Y.-W.; Pang, X.-Y.; Delmon, B. *J. Phys. Chem. A* **2000**, *104*, 11375.

(21) Ma, X.; Schobert, H. H. *J. Mol. Catal. A: Chem.* **2000**, *160*, 409.

(22) Orita, H.; Uchida, K.; Itoh, N. *J. Mol. Catal. A: Chem.* **2003**, *195*, 173.

(23) Calais, C.; Matsubayashi, N.; Geantet, C.; Yoshimura, Y.; Shimada, H.; Nishijima, A.; Lacroix, M.; Breysse, M. *J. Catal.* **1998**, *174*, 130.

(24) Orita, H.; Uchida, K.; Itoh, N. *J. Mol. Catal. A: Chem.* **2003**, *193*, 197.

(25) (a) Delley, B. *J. Chem. Phys.* **1990**, *92*, 508. (b) Delley, B. *J. Phys. Chem.* **1996**, *100*, 6107. (c) Delley, B. *J. Chem. Phys.* **2000**, *113*, 7756.

(26) Delley, B. *Phys. Rev. B* **2002**, *66*, 155125.

(27) Perdew, J. P.; Wang, Y. *Phys. Rev. B* **1992**, *45*, 13244.

(28) Spirko, J. A.; Neiman, M. L.; Oelker, A. M.; Klier, K. *Surf. Sci.* **2003**, *542*, 192.

(29) (a) Diez, R. P.; Jubert, A. H. *J. Mol. Struct.* **1990**, *210*, 329. (b) Delannay, F. *Appl. Catal.* **1985**, *161*, 135. (c) Startsev, A. N.; Zaikovskii, V. I. *Kinet. Katal.* **1994**, *35*, 288.

(30) Muramatsu, A.; Tatsumi, T.; Tominaga, H. *J. Phys. Chem.* **1992**, 96, 1334.

(31) Li, Z.; Fu, Y.; Bao, J.; Jiang, M.; Hu, T.; Liu, T.; Xie, Y.-N. *Appl. Catal., A* **2001**, *220*, 21.

(32) (a) Loaiza-Gil, A.; Fontal, B.; Rueda, F.; Mendialdua, J.; Casanova, R. *Appl. Catal., A* **1999**, *177*, 193. (b) Cubeiro, M. L.; Morales, H.; Goldwasser, M. R.; Pérez-Zurita, M. J.; González-Jiménez, F.; Urbina de N, C. *Appl. Catal., A* **1999**, *189*, 87. (c) Bukur, D. B.; Koranne, M. K.; Lang, X.; Rao, K. R. P. M.; Huffman, G. P. *Appl. Catal., A* **1995**, *126*, 85. (d) Bukur, D. B.; Lang, X.; Rossin, J. A.; Zimmerman, W. H.; Rosynek, M. P.; Yeh, E. B.; Li, C. *Ind. Eng. Chem. Res.* **1989**, *28*, 1130. (e) Bukur, D. B.; Okabe, K.; Rosynek, M. P.; Li, C. P.; Wang, D. J.; Rao, K. R. P. M.; Huffman, G. P. *J. Catal.* **1995**, *155*, 353. (f) Bukur, D. B.; Nowicki, L.; Manne, R. K.; Lang, X. S. *J. Catal.* **1995**, *155*, 366. (g) Bukur, D. B.; Nowicki, L.; Patel, S. A. *Can. J. Chem. Eng.* **1996**, *74*, 399.

(33) Cao, D.-B.; Zhang, F.-Q.; Li, Y.-W.; Jiao, H. *J. Phys. Chem. B* **2004**, *108*, 9094.